A mummy's secrets: Serendipity, Computed Tomography and non-invasive x-ray diffraction

S.R. Stock*
Dept. of Cell and Developmental Biology, Feinberg School of Medicine,
and Simpson Querrey Inst., Northwestern Univ., Chicago, IL, USA

ABSTRACT

Contents of a Roman-era Egyptian mummy (Hawara portrait mummy 4, HPM4) were investigated by clinical Computed Tomography (CT) and position-resolved, high-energy, microbeam x-ray diffraction at the Advanced Photon Source (APS). The combined techniques provide a more complete picture of the mummy than either could alone. From CT, the person within the mummy was about five years old at death, there was no evidence of skeletal trauma and the team inferred female biological sex. Other foci of the CT investigation were moderate absorption shards within the skull cavity, identified as resin; the layers of linen wrapping the mummy, in particular one layer which appeared to be heavily impregnated with bitumen or pitch; wires (specimen pins) apparently added during earlier restorations of HPM4 and a large, high attenuation inclusion located in the wrappings above the abdomen. The CT data also provided a 3D "roadmap" guiding the diffraction experiments, the first of their kind performed in situ on an intact mummy. A ray tracing technique was developed to identify where along the x-ray beam path diffraction signals originated, and in all of the cases, precision were 1-2 mm. Further, the diffraction origins matched positions of these features in the CT scan. Diffraction identified the wires as modern dual phase steel matching that of a reference specimen pin and the inclusion above the abdomen as calcite, possibly a carved scarab. The cross-sections of the skull and of the femora were mapped accurately with the technique, but the desire to minimize potential beam damage to HPM4 dictated that very short integration times were used and the signal to noise ratio was too low for detailed analysis of the bone diffraction patterns. The CT plus diffraction approach to studying the contents of mummies adds very important information, but the logistics of transporting a mummy first to a CT scanner and then to a synchrotron radiation source mean that the approach will probably only be used to solve key mysteries.

Keywords: Egypt, mummy, Computed Tomography, x-ray diffraction, high energy x-rays, synchrotron x-radiation

1. INTRODUCTION

In late November 2017, a Roman-era Egyptian mummy (Hawara portrait mummy 4, HPM4) traveled to the Advanced Photon Source (APS), and contents of the mummy were investigated using position-resolved, high-energy x-ray diffraction. The diffraction experiments were guided by previously recorded Computed Tomography (CT) scans. How this came to happen is one of the main threads of this paper, the other being the results obtained. Perhaps the most striking feature of the study was the number of instances of serendipity leading to the diffraction experiments.

During 2016, the Block Museum, Northwestern University, was planning an exhibit "Paint the Eyes Softer" on portraits from Egyptian era mummies. A number of interdisciplinary studies of the portraits were envisioned involving multiple units of Northwestern and several undergraduate courses; student design was to be integral part of aspects of the exhibit. One of the exhibit curators went to the Styberg Library of the Garrett-Evangelical Theological Seminary to consult a reference book. As shown in Fig. 1a, Garrett is surrounded by Northwestern's Evanston campus, is but a short walk from the Block Museum and is an institution independent from Northwestern. Within a glass case near the entrance door of the Styberg Library, HPM4 was displayed for viewing by anyone entering the library (Fig. 1b). The portrait mummy was recognized as closely related to the portraits to be included in the exhibit, and the decision was made to include HPM4 as the exhibit's final display.

At the time HPM4 was "found", it was still heavily encrusted with soil, and the soil and ambient humidity appeared to be damaging the linen wrappings of the mummy. The decision was taken to stabilize HPM4 by removing the soil and to use a clinical CT scanner to look for subsurface degradation. As described below, that is when the author was consulted for

* s-stock@northwestern.edu

Developments in X-Ray Tomography XIII, edited by Bert Müller
Ge Wang, Proc. of SPIE Vol. 11840, 1184003 · © 2021 SPIE
CCC code: 0277-786X/21/$21 · doi: 10.1117/12.2603691

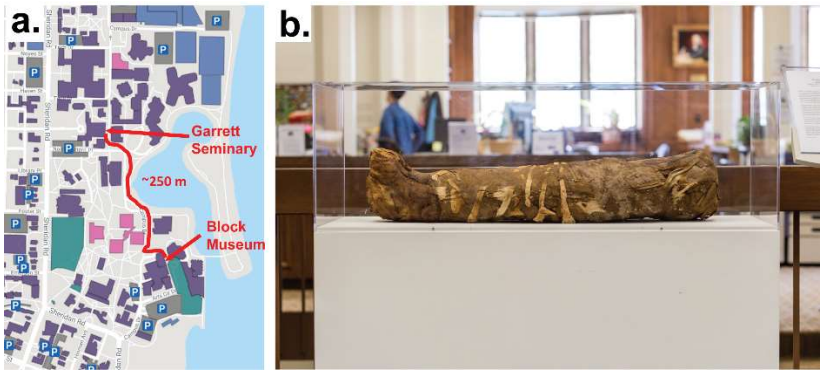

Fig. 1. (a) Map from the Northwestern University website showing the proximity of the Block Museum and the Styberg Library, Garrett-Evangelical Theological Seminary. (b) Photograph of Hawara Portrait Mummy 4 just inside the front door of the Styberg Library and prior to conservation.

his help getting the CT scan completed prior to conservation. X-radiographs collected in the 1960s showed unknown radiodense ellipsoidal objects within the linen wrappings, and a CT scan would only show how absorbing the objects and would not identify the materials because minerals such as malachite, jasper and calcite produce virtually indistinguishable CT contrast. X-ray diffraction can identify different materials, and, if high energy x-rays are used, x-ray diffraction can non-invasively peer inside large objects such as mummies. The author lobbied for permission to take HPM4 to APS and to perform position-resolved, x-ray diffraction. The author obtained permission, one day of beam time was scheduled before conservation was complete, HPM4 was transported to APS, the diffraction mapping was performed, HPM4 was returned for completion of conservation, HPM4 was exhibited (Jan 13-April 22, 2018) and the conserved HPM4 resumed its place in Styberg Library after the exhibit ended.

It is interesting to note that Flinder's excavation of HPM4 (1910-1911)[1], Laue's discovery of x-ray diffraction (1912)[2], Bragg's formulation of the eponymous law (1912)[3] and Radon's demonstration of the mathematics underlying computed tomography (1917)[4] all occurred within seven years. The tone and topics of this paper differ from the typical SPIE conference proceedings papers as it includes much about of how the measurements came to be performed and involves the author's personal observations. The volume describing the exhibit[1] gathered considerable background information, and the different chapters are cited below.

1.1 Egyptian funerary practices and mummies[5]

Mummification, as a means to preserve bodies so that the deceased's spirit would have a vessel in the afterlife, was practiced for millennia in ancient Egypt. Thoracic and abdominal organs were removed through an incision in the abdomen, and the brain through a hole punched through one of the nostrils. After artificial desiccation using a natural salt mixture called natron, the bodies were then wrapped in strips of linen. Later, in Roman times, resin and bitumen were used as preservatives. Until the Roman conquest of Egypt (30 BCE), mummified remains were placed in sarcophagi bearing decorative painting, and funerary masks, termed cartonnage, were placed over the head of wrapped bodies. These masks were painted in a highly stylized fashion showing basic human physiognomy in 3D but no individuality. Early in the Roman period, the depiction of the person within the wrappings shifted dramatically. Impersonal cartonnage was replaced by much more realistic and individualized 2D paintings on linen or on thin panels of wood, i.e., an incorporation of Hellenic artistic methods. The incorporation of portraits on mummies continued until the adoption of Christianity as the state religion (395 CE), and the surviving mummy portraits are perhaps the most comprehensive record of the Hellenic painting tradition. Only about 10% of the slightly more than 1,000 mummy portraits known to exist are still attached to their mummies, and this makes HPM4 an exceedingly rare artifact.

1.2 From Egypt to London to Evanston[6]

Flinders Petrie and his team excavated HPM4 and four other mummies from a funerary chamber during their 1910-1911 expedition season. The site was in the cemetery at Hawara a few miles away from the source of most of the portraits included in the Block Museum exhibit. At the end of the season, some of the finds went to the Egyptian government and Petrie's share was transported to London (including HPM4, other mummies and many other artifacts) for exhibition,

cataloging and distribution to various institutions supporting the expedition. One major financial supporter was Mrs. Lydia Hibbard, the widow of William "Gold" Hibbard who ran a large hardware wholesaling company in Chicago (its revenue in 1867, for example, was reported at over one million dollars). Petrie's records indicate the Mrs. Hibbard was to receive a portrait from one of the mummies and the Oriental Institute Museum of the University of Chicago was to receive HPM4. Instead, Mrs. Hibbard (of Chicago) received HPM4 and the Oriental Institute the portrait. Although it was likely that a shipping or clerical error led to the switch, a movie fictionalization would probably depict some sort of shenanigans typical of Chicago leading to the diversion of HPM4, perhaps at the behest of an eminence grise at Northwestern University who wished to prevent the academic cross-town rivals (University of Chicago) from possessing this treasure. Some decades later when the definitive catalog of portrait mummies was produced, this switch meant that HPM4 could not be found where it was supposed to be and it was "lost" to Egyptologists. In actuality, Mrs. Hibbard donated HPM4 to the library of Western Theological Seminary in 1912 so that HPM4 could help broaden the Old Testament background of clergy in training. In the 1930s, the Western Theological Seminary and Seabury Seminary merged at a single location in Evanston, across Sheridan Rd. from Garrett-Evangelical Theological Seminary and adjacent to Northwestern University. Some further decades later, Seabury-Western closed its Evanston doors with Northwestern buying the buildings and Garrett the library. In the movie version of events, Northwestern's eminence grise would have thereby acquired physical control of HPM4. In reality, HPM4 remained "lost," except to the seminary community, until the 1980s when it was added to the catalog of known portrait mummies. It is important to note that the Northwestern community was totally unaware of the presence of this portrait mummy in the middle of its Evanston campus.

1.3 A series of fortunate events

In the summer of 2016, a conference "Synchrotron Radiation and Neutrons in Art and Archaeology (SR2A)" was to be held at The Art Institute, Chicago. At the time, the author was working on a microCT and synchrotron x-ray diffraction study of human archeological second metacarpal bones. One of the organizers (Carmen Soriano, then working at APS) was a collaborator and personal friend of the author and suggested that the author's metacarpal study might be of interest to the attendees. The location near to the author's home institution was a positive, and he submitted an abstract. The abstract was accepted as a poster presentation, and, as the author hates giving posters and would have to pay the registration fee out of his own pocket, he seriously considered withdrawing the abstract. In the end, the personal relationship won out and the author prepared and presented his poster. There was a remarkable lack of interest by the attendees; however, the osteoarchaeological community has since positively reviewed the results. At the meeting, the author talked to Marc Walton one of the organizers of SR2A, and Walton learned of the author's expertise in CT imaging.

Walton specializes in analysis of portraits from Roman era Egyptians mummies and was one of the curators for the Block Museum exhibition mentioned above. The exhibit was being organized when Essi Rönkkö, a participating curator from the Block, walked by HPM4 in the Styberg Library of Garrett-Evangelical Theological Seminary. Loan was arranged for the exhibit, and Walton contacted the author to arrange the CT imaging at Northwestern Memorial Hospital. Once the CT scan was complete, the author arranged x-ray diffraction measurements on the mummy's contents at APS, Argonne National Laboratory, an hour's drive from Evanston. Throughout, the research and exhibition plan involved "vertical integration" within Northwestern University, i.e., making use wherever possible of Northwestern students, staff and researchers.

1.4 The exhibit, its contexts and questions

Several aspects of HPM4 and its various contexts were of especial interest for the exhibit and for the related scientific investigations. The first context is that of the individual within the mummy: the biological sex, any anatomical abnormalities, age at death and cause of death. There was speculation in the 1960s that HPM4 contained crocodile remains and not human remains, and radiographs were recorded and revealed that the mummy was human.[6] Earlier CT data from 2000, the reconstructed slices of which were sadly recorded only on radiographic film, was at much lower resolution than is presently possible and gave only a determination of age at death (about 5 years) and sex (female).[7] The current CT study was intended to confirm the earlier observations and to document any in vivo abnormalities or skeletal trauma. The second context is the evidence of the mummification process contained within the body and wrappings of the body, including object purposefully or accidentally enclosed in the wrappings. In particular there is a large ellipsoidal object in the wrappings of above the abdomen. The third context is the evidence of post-excavation changes to HPM4, either environmental degradation or repairs to the linen layers.

A preliminary report of the studies on HPM4 appeared in the exhibit volume[8] and a fuller report in the archival literature.[9] The methods and the principles underlying these methods are covered briefly below, and the CT and x-ray diffraction results are presented as well. Implicit in the statement of the three contexts are a number of questions, and the extent to which these were answered is one focus and a second is what improved methods might allow us to learn in the future.

2. MATERIALS AND METHODS

In August 2017, HPM4 was packed in a special crate and transported to Northwestern Memorial Hospital by specialist art transporters. Throughout, HPM4 was kept on a custom-built tray which allowed the 20-25 kg mummy to be moved without actual contact with its surface. In the CT room, the crate was unpacked (Fig. 2a), and HPM4 was lifted by the tray and placed on the scanner bed (Fig. 2b). After a short while at the hospital, the mummy was returned to an Evanston lab where the conservation and student projects were to be conducted. The author obtained 24 hours of beam time through an APS General User Proposal, and the diffraction experiments were scheduled for the Monday after the US Thanksgiving Day holiday weekend, in order to allow the assembly of an unusual translation system capable of accommodating the mummy's weight and covering moving 1.2 m horizontally and 200 mm vertically. Experimental safety forms for the APS experiment were filed well in advance. On the afternoon of the last working day before Thanksgiving, the author received a query from Argonne National Laboratory about bringing human remains on site. The author explained the human remains were within a mummy and would not be disturbed nor pose a hazard, and this potential roadblock was resolved. The mummy arrived, via the art transporters, at about 6 am of the morning of the experiment, and was placed on the translation stage in the next couple of hours. Beam was stored and available for experiments at 8 am. There was considerable press activity until 1 pm although some alignment scans were completed. Scanning at different positions ran until about 6:30 am the next day. By 8 am, HPM4 was removed from the translation stage, packed in its shipment crate and on its way back to the lab in Evanston. About this time, the author received an e-mail from a retired colleague who saw, over his morning cup of coffee, that the mummy story was featured above the fold on the front page of the Chicago Tribune (November 28, 2017).

2.1 Computed Tomography

Computed Tomography was performed at Northwestern Memorial Hospital using a Siemens SOMATOM Force system (Fig. 2b). Two scans were recorded of HPM4, one with 0.82 mm in-plane and 1.0 mm out-of-plane volume elements (voxel) and a second with 0.69 mm in-plane and 1.00 mm out-of-plane voxels; the former was used to select features for position-resolved x-ray diffraction, the latter for 3D renderings. Features selected for x-ray diffraction analysis were: wires in the wrappings near the skull, the skull, resin shards within the skull, teeth, cervical vertebrae, femora, inclusions A and D (which have similar contrast, D is not shown in the CT data) and inclusion F. As is conventional for clinical scanners, x-ray attenuation values were quantified in Hounsfield units (HU), linear attenuation coefficients expressed in a scale with distilled water equaling 0 HU and air -1000 HU. Cortical bone is typically 1400-1700 HU and human enamel 2500-2800 HU.[10] Visualization and rendering used Amira 6.4 (FEI Visualization Sciences Group, Berlin, Germany). Most segmentation could be done by simple selection of contrast levels, but one wrapping layer with relatively high absorptivity (Results) required manual segmentation.

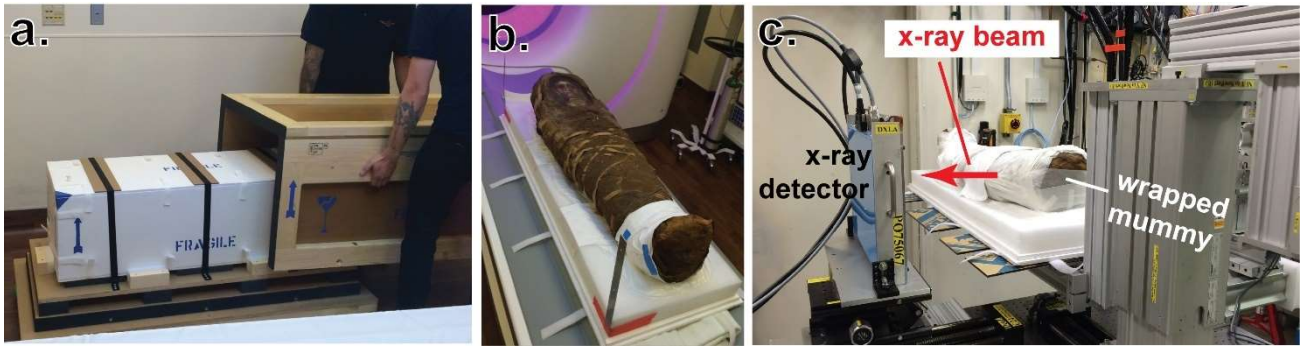

Fig. 2. (a) Transport crate and unpacking prior to CT imaging. (b) HPM4 on its transport tray placed on the CT scanner platform. The platform will translate HPM4 away from the viewer and into the scanner (purple lit open area underneath the panel label "b"). (c) HPM4 in place for x-ray diffraction at beamline 1-ID, APS. The mummy was wrapped in white tissue to protect it from contamination.

2.2 X-ray diffraction scans

Transmission x-ray diffraction patterns were collected at beamline 1-ID (Fig. 2c, 3a), APS, using 71.676 keV photons and a $(0.25\ \text{mm})^2$ wide microbeam. Most of the details of the experiment are reported elsewhere.[9] The x-ray area detector (Dexela 2923 CMOS detector; 3888 x 3072 pixels, 75 μm pixel pitch) was nominally perpendicular to and centered on the incident x-ray beam and mounted on a translator allowing the specimen – detector separation to be varied. Using the 3D CT roadmap, diffraction patterns covered the objects of interest by translating HPM4 vertically and horizontally across the beam. Collecting each pattern required 4 s (0.2 s pattern collection time). Coordinate axis Z was along the beam direction; axes X and Y were perpendicular to Z and were along the horizontal and vertical directions, respectively.

Diffraction patterns consisted of complete or incomplete diffraction rings and discrete diffraction spots. The crystal periodicities d_{hkl} (d-spacings) were determined from the angles $2\theta_{hkl}$ at which each $hk.l$ diffracted beam makes with the incident beam via Bragg's law: $\lambda = 2\ d_{hkl} \sin\theta$, where λ is the x-ray wavelength and θ is the Bragg (diffraction) angle. Note that period in the indices indicates the Miller-Bravais indexing system[11] to emphasize the hexagonal crystal system. When area detectors record transmission x-ray diffraction patterns, the separation between diffracting volume and detector must be known for the diffraction angle to be calculated. Figure 3b illustrates a complication of large paths through specimens such as HPM4: At detector position 1, diffraction peaks might be from anywhere between positions A and B; angular and d_{hkl} uncertainties are too large to be useful. Repeating the measurement with the detector 400.0 mm farther away (position 2) resolves the ambiguity, identifies the depth originating the diffracted beam and provides an accurate d_{hkl}.

A diffraction-based alignment scan along X at $Y = 0$ located the crown of the skull (bone diffraction patterns appeared). Next, Y-scans across the skull at $X = 111$ mm and 100 mm ensured that the vertical translation range covered the expected positions of the resin shards, wires near the skull, teeth, femora, cervical vertebrae, inclusions F, A and D. Scans across all of the regions of interest were performed at detector position 1 and then at detector position 2, 400 mm farther from HPM4 than position 1. The diffraction patterns were collected as a series of Y-scans (translation increment $\Delta Y = 0.5$ mm or 1 mm and ~130 patterns per Y scan) at 5-7 X positions. The X positions were selected based upon the objects' distance from the crown in the CT scan. Between scans at detector position 1 and 2, diffraction patterns were recorded at both detector positions of reference materials (an archeological human bone, a second metacarpal, mc2, and a steel insect pin thought to be similar to the wires inserted into the wrappings) placed beyond the cranial end of the mummy.

After detector tilt correction, the 2D polar geometry diffraction patterns (diffracted intensity vs radii r) were converted to Cartesian plots I (r, η): circular Debye rings covering all azimuths η transformed to lines, and discrete spots at a specific η remained spots at that η. From the radii and the known detector translation (400.0 mm), extrapolation to $r = 0$ revealed the Z position originating the diffracted intensity. With Z known, 2θ is calculated from trigonometry and d from Bragg's law. The series of d from the same X,Y,Z are characteristic of the crystallographic phase(s) present, and phase identification was done using the Powder Diffraction File (PDF), a database of experimentally-determined polycrystalline diffraction patterns.[12]

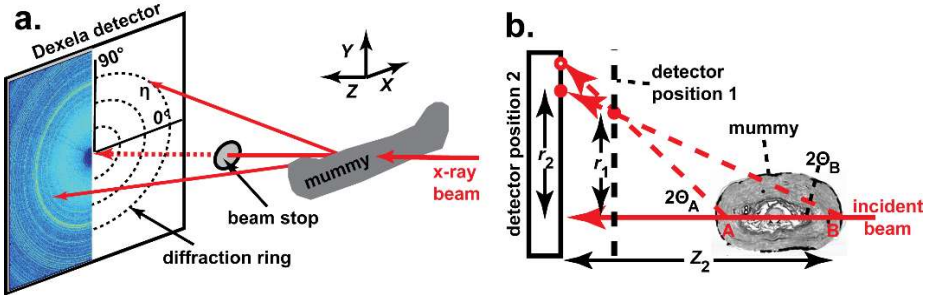

Fig. 3. (a) Schematic of the diffraction set-up at beamline 1-ID, APS. The incident x-ray microbeam passes through the mummy and is blocked by the beam stop before it hits the detector. When the incident beam traverses polycrystalline objects within the mummy, cones of diffracted intensity result and are recorded on the area detector. (b) Schematic of the complication in the transmission geometry of a long path through the mummy. A diffraction peak observed at the position of the red disk (r_1 away from the incident beam position) at detector position 1 might originate at any position between A or B. The possible diffraction angles 2θ could range between $2\theta_B$ and $2\theta_A$. The same diffraction peak recorded at r_2 (red disk) and not at the position of the open red circle would show that the beam originated from position B. The precise 2θ value determines d accurately enough to identify the material diffracting at position B. Adapted from [9].

3. RESULTS AND DISCUSSION

The first two sub-sections provide an overview of the CT and diffraction data for HPM4. The third covers the questions of age at death and biological sex of the individual within the mummy. The fourth and five describe the biological tissues, the skull and femora. The sixth through ninth sub-sections present and interpret results on the low attenuation shards within the cranial vault, the layers of linen, wires and inclusion F. The final sub-section covers lessons learned about the conduct of CT-guided, position resolved diffraction of mummies and possible further studies.

3.1 Overview of the CT data

Figure 4 shows CT slices through the skull, a cervical vertebra and the abdomen of HPM4 and identifies several (but not all) features investigated in this study. In Fig. 4a, features of importance in the diffraction analysis include the resin shards "rs", the skull "s", soil "so" and one of the many wires "w". The cervical vertebra "cv" and layers "ℓ1" and "ℓ2" are labeled in Fig. 4b and radius and ulna "r, u" and inclusion F ("incl F") in Fig. 4c. The portrait "p" and inclusion A ("Incl A"), which was not detectable by diffraction, are not discussed further.

Figure 5 shows 3D renderings of HPM4 with different internal features rendered in different colors. These features are discussed in separate sub-sections below. The skeletal length is 937 mm with wrappings adding another 50 mm. The maximum mediolateral width of HPM4 equals 285 mm at the shoulders; the maximum anteroposterior thicknesses are 179 mm at the head and 202 mm at the feet.

3.2 Overview of the diffraction data

Diffraction patterns from various objects within HPM4 differed dramatically, reflecting the characteristics of the materials producing the patterns. Figure 6a shows a diffraction pattern from inclusion F; it is in the "native" 2D format of the area detector, polar plot of diffracted intensity as a function of radius *r*. Different diffraction peaks escribe arcs or circles of constant *r*, as described below, the peaks from inclusion F are continuous and have a narrow radial width, and the scattered spots are from soil on the surface of the mummy. Figure 6b is from the skull and has been transformed into a Cartesian representation of the diffraction pattern. As is discussed below, the diffraction peaks indicated the pairs of arrows are from either side of the skull, the two sides being displaced far enough along the beam direction *Z* that the 00.2 (red arrows) and quadruplet (yellow arrows, indices given below) carbonated apatite (cAp) reflections split apart. Note that the azimuthal intensity variation of the 00.2 peaks is much greater than that of the quadruplet reflections. Figure 6c shows a longitudinal section through HPM4 with the positions of the *Y*-scans covering the features described in subsequent subsections. Scan position 1 covered the skull and wires, 2 covered inclusion F and 3 covered the femora.

Figure 7 shows Cartesian plots of diffraction patterns from the same position but at the two detector distances. The letters denote discrete spots, and the numbers diffraction lines. The patterns are screen captures from ImageJ which was used to manually measure the position of each feature. When matching spots (or lines) at the two detector positions, the relative radial positions may change, depending the *Z* position and the values of 2θ, but the azimuth angle of the feature is invariant

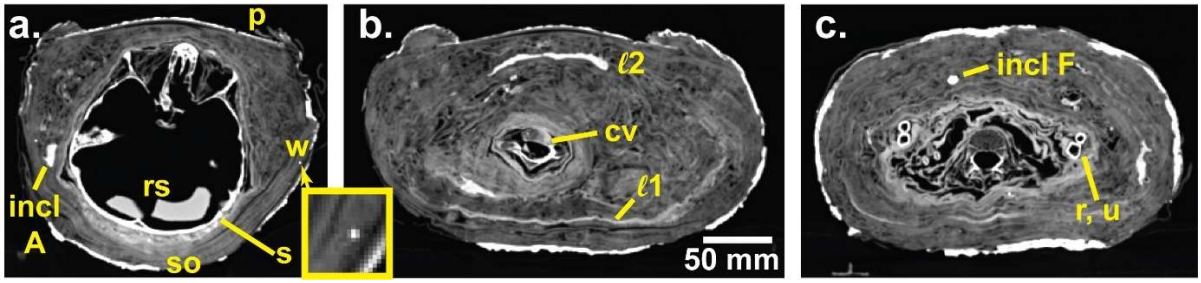

Fig. 4. Three CT slices through HPM4; the anterior surface of the mummy is up in these images. White contrast indicates area of higher x-ray absorption. (a) Slice through the skull with labels: Inclusion A "incl A", skull "s", soil "so", resin shards "rs", portrait "p" and wire "w". An enlargement of the area around the wire is shown within the inset yellow box. (b) Slice through a cervical vertebra "cv" with dense linen layer ℓ1 and layer ℓ2 identified. (c) Slice through the abdomen with high absorption inclusion F within the abdomen's wrappings and radius and ulna labeled "incl F" and "r, u", respectively. The scale bar applies to all three images. Adapted from [9].

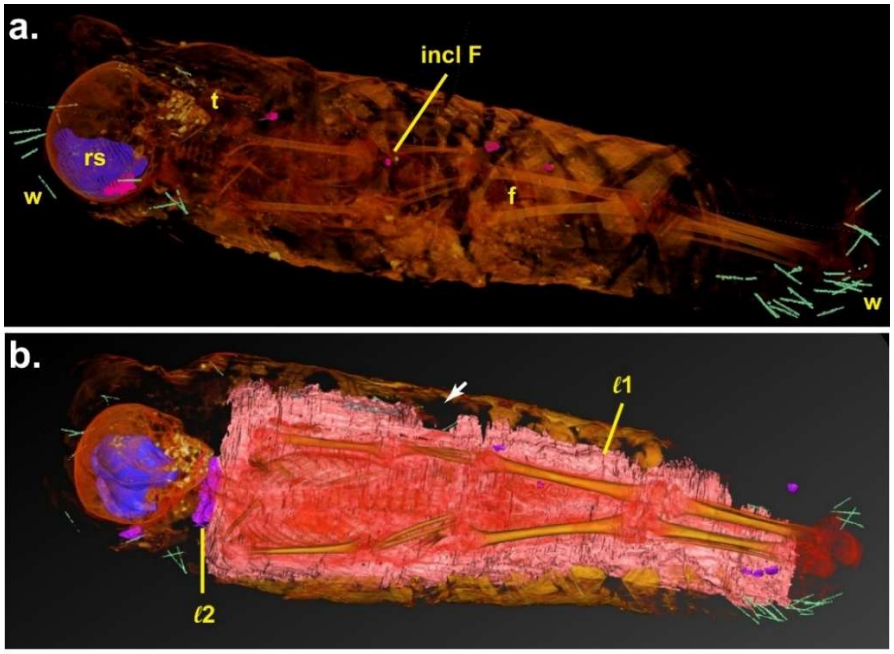

Fig. 5. Two 3D renderings of HPM4 with labels matching those in Fig. 4; the skeletal length is 937 mm (from the crown of the skull, left, to the bottom of the feet, right). (a) The wrappings, bone and teeth "t" are shown semitransparent with darker yellow shades indicating higher attenuation. Wires are rendered green, the resin shards are colored blue and various objects within the wrapping but having higher linear attenuation coefficient values are shown in magenta (including inclusion F "incl F"). (b) The mummy from a slightly different viewing angle than in the first panel. The bones and teeth are rendered in the same yellow color scale as in (a), the long bones (femora, tibiae, fibulae, etc.) and teeth are rendered opaque, and the front surface of the wrappings has been removed. The dense layer posterior to the skeleton ("l1" in Fig. 4b) is rendered pink and extends from shoulders to ankles and partway up the sides; layer "l2" is rendered magenta. The highly absorbing inclusions within the wrappings (above the torso and legs) appear purple. Wires are shown in green, and the white arrow shows wires which were not visible in (a). Adapted from [9].

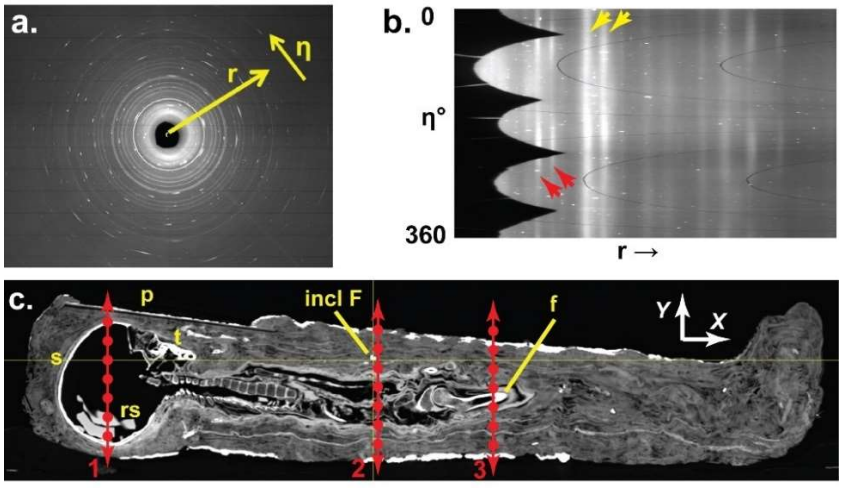

Fig. 6. (a) Diffraction pattern of inclusion F as recorded on the 2D area detector. Radius *r* and azimuth η are indicated. (b) Diffraction pattern from the skull with the red and yellow pairs of arrows indicate the 00.2 and quadruplet carbonated apatite reflections, respectively, from the two sides of the skull. The lighter the pixel in the diffraction patterns, the higher the intensity. The scalloping (missing intensities) at the left is an artifact of the mask used to remove the low angle scatter. (c) Longitudinal CT image of HPM4 with positions indicated of the diffraction scans across features discussed below. Symbols are the same as in preceding images. The lighter the voxel, the greater the x-ray absorptivity. Adapted from [9].

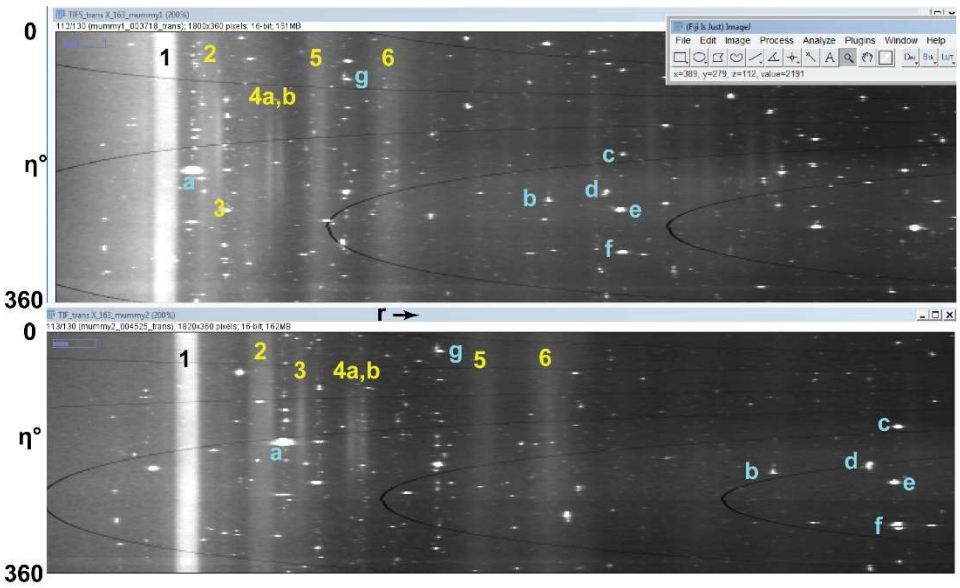

Fig. 7. (top) Cartesian plots of diffraction patterns recorded at the same *X,Y* position but with detector position 1 (top) and 2 (bottom). The numerals identify diffraction lines (from bone) and the letters discrete diffraction spots. Radius *r* and azimuth η are indicated.

and the shape of the feature typically does not change. If this approach were to be used again, machine learning might make it practical to measure more features than were extrapolated in this study.

3.3 Age at death and sex[9]

The CT data show all bones are present and well-preserved in HPM4 and remain articulated in anatomical position. The anterior cranial fossa is pierced, connecting the nasal and cranial cavities, a common but not universal procedure in Egyptian mummification.[13] Otherwise, skeletal trauma is absent, leaving cause of death indeterminate. Deciduous dentition is complete, none of the permanent teeth have erupted and the crown enamel of the first and second permanent molars is partially developed. Tooth development data[14] indicates that age at death was approximately 5 years (± 0.75 yr). Soft tissue of HPM4 were well preserved although shrunken. Male external genitalia could not be seen, something which can be observed in similarly well-preserved mummies of boys of the same age,[15] and some of the external soft tissue could be labia (external female genitalia). This led the author and colleagues to infer that a five year old girl lies within the mummy,[9] a conclusion confirming age and sex determination published earlier.[7]

3.4 Skull

Figure 5a shows the skull's sides reach thicknesses up to 3-4 mm, but the bone is typically thinner than this. The maximum attenuation is 1,250 ± 190 HU (mean ± one standard deviation). Bone is a composite consisting primarily of collagen and cAp, and the cAp 00.2 and quadruplet "q" (unresolved 21.1, 11.2, 30.0 and 20.2) reflections (see Fig. 6b) are the only peaks from the skull with appreciable intensity. As mentioned above, the x-ray beam traverses both the left and right sides of the skull, and these positions are far enough apart that their diffracted beams separate on the x-ray detector. Figure 8, at *Y*-scan position 1 (Fig. 6c), shows Cartesian plots of portions of six skull patterns containing 00.2 and q reflections. The value of *Y* at which each pattern was recorded is in the upper left of each panel. At $Y = -63$ mm, the beam is hitting the most anterior portion of the skull, and only one 00.2 and one q reflection are visible and the intensities of these reflections are weak. At $Y = -62$ mm, only 1 mm further into the skull, the 00.2 reflection has broadened; at $Y = -59$ mm, separate reflections are well resolved from the skull's two sides. At $Y = -50$ mm, the pairs of 00.2 and q reflections have moved farther apart. By $Y = -32$ mm, the 00.2 peak from one side of the skull is overlapping with the q reflection of the other side, and by $Y = -1$ mm, one q peak appears at a lower radius than one of the 00.2 peaks.

When one traces the 00.2 reflections back to their origin within the mummy, Fig. 9a results. The slice image in Fig. 9b is at approximately the same position as the Y-scan in Fig. 9a, but is at a slightly different magnification and appears tilted

relative to Fig. 9a. The average over many points in the skull is $d_{00.2}$ = 3.430 Å which is similar to that of synthetic hydroxyapatite (hAp, $d_{00.2}$ = 3.4325 Å, PDF 00-086-1201). Integration times for these diffraction patterns was kept much lower than is typically the case at 1-ID, mainly to limit the x-ray dose. The resulting signal to noise in the patterns from the skull (and from the femora described in the next sub-section) was adequate for extrapolation to originating voxel and to observe crystallographic texture (i.e., the azimuths above and below the red arrows for the cAp 00.2 diffraction lines in Fig. 6b) but was inadequate for the analyses typically done for bone cAp (i.e., precision peak position measurements for lattice parameter quantification; peak width analysis for determination of crystallite size and microstrain).

3.5 Femora

Figure 10a shows a CT slice through the femora. In this slice, cortical thickness is ~3 mm, and the medial-lateral and anterior-posterior outer diameters average 15-16 mm (femur 2) and 13 mm (femur 1). The anterior-posterior gap between femora is ~5 mm. Linear attenuation coefficients approach 1,500 ± 135 HU, slightly larger those for the skull. The cAp diffraction patterns were similar to those of the skull ($d_{00.4}$ = 1.728 Å roughly matching hAp) and showed similar, albeit smaller, splitting of 00.2 diffraction lines. For femur 1, cAp diffraction patterns were seen over 12 mm in *Y*; there was a gap of 5 mm without cAp patterns and, for femur 2, cAp patterns were observed over 13 mm.

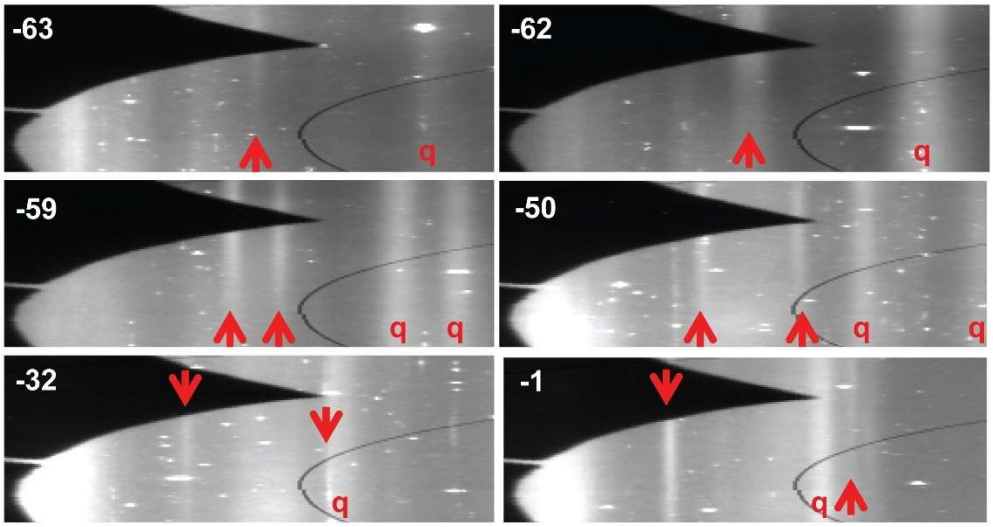

Fig. 8. Portions of six diffraction patterns covering the 00.2 and q reflections (vertical = azimuth; horizontal equals radius). All patterns were recorded at the same *X* position, and the number in the upper left corner of each panel gives the *Y* position at which each pattern was recorded. The arrow heads show 00.2 reflections and "q" labels the quadruplet reflection (unresolved 21.1, 11.2, 30.0 and 20.2 peaks). The section numbers appear above the left corner of each image.

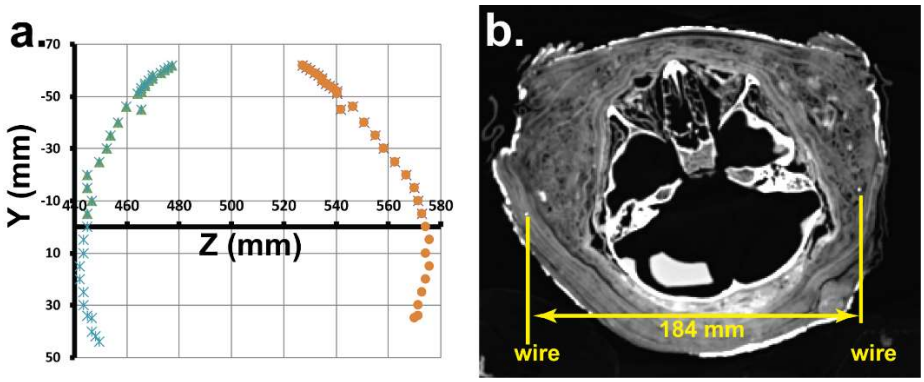

Fig. 9. (a) Origin of cAp diffraction peaks determined for the skull. (b) CT slice of the skull at the approximate position mapped in panel a. There is a slight difference in tilt and scale between the two panels. The information on the wires in yellow is discussed in a subsequent sub-section. Adapted from [9].

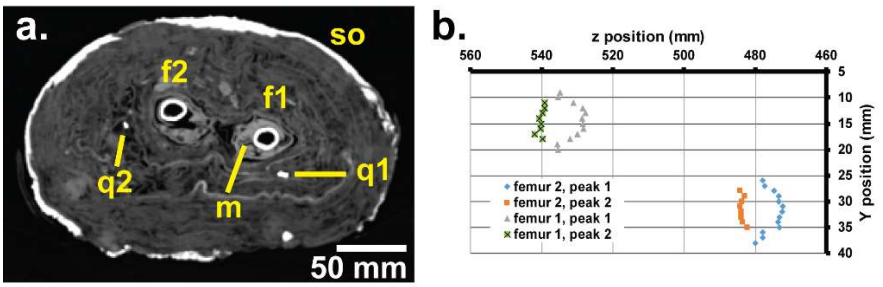

Fig. 10. (a) Slice showing femora f1 and f2, muscle tissue "m", soil "so" and two high absorption particles describe in a later sub-section. (b) Origins of cAp diffraction from the femora determined from the extrapolation method. Peak 1 and peak 2 refer to the two sides of the femora. Note that (a) and (b) are at slightly different magnifications. Adapted from [9].

Figure 10b shows the origins of cAp diffraction lines. The diffraction-determined femoral diameters, mediolateral femoral separation and the anteroposterior femoral separation match those seen in the CT slice. Note that there is some uncertainty in orientation between the tray positioning in the CT scanner and that on the diffraction translator. Inspection of Fig. 10b reveals that origins at the anterior and posterior edges of both femora consists of two or three nearly identical single origin points despite the translation. The cAp 00.4 reflections at these points have not separated enough for the medial and lateral cortices to be resolved. Evidently, with this experimental set-up, separations of ΔZ~5 mm are required before separate objects (medial, lateral cortices) can be resolved.

3.6 Low attenuation shards within the cranial vault

Low absorption shards are prominent within the skull vault (Fig. 4a) and have very uniform attenuation (115 ± 17 HU), considerably greater than air (– 990 ± 3 HU) and matching published values[10] for resin in mummies (71 ± 23.4 HU). The shards are quite curved and have uniform thickness of 10-11 mm. Virtual assembly of the shards shows they are an endocast of the region surrounding the cruciform eminence.[16] The shards are an unusual endocast. Resin solidified in skulls of most Egyptian mummies with the body lying supine[13, 17, 18] although that of Tutankhamun shows two orientations[19].

If the shards were intercepted by the x-ray beam it would have been at the bottom of the Y-scans of the skull. At these positions, neither diffraction (aside from cAp diffraction lines of the skull and sharp spots extrapolating back to the mummy surface) nor a large increase in background scattering (which would occur when the amount of non-crystalline material increased) were observed. The author concludes that the scans did not reach the shards. Because absorption values match published CT values and resin was used as a preservative when HPM4 was produced, the shards were identified as resin which solidified as the body was tilted continuously, a procedure that has not been documented previously.[9]

3.7 Linen layers

Layers of linen can be resolved in many locations within HPM4 but are frequently too closely spaced for individual layers to be distinguished (Fig. 4, 6c, 9b, 10a). The layers' mean linear attenuation coefficient is -540 ± 95 HU vs -990 HU for air and 115 for the shards. Although HPM4 is tightly wrapped, the space between the linen layers and within the weave produces the relatively large standard deviation. Dense layer 1 (ℓ1, Fig. 4b) within the linen wrappings (-65 ± 95 HU) follows the contours of the body (Fig. 4b) and spans the majority of the body's dorsal surface and as well as its right and left sides (Fig. 5b). Layer ℓ1 is continuous but contains small gaps often where the layer appeared thin in adjacent slices. Attenuation values of layer ℓ1 suggest it is linen heavily impregnated with resin/bitumen. The function of layer ℓ1, if any, is unknown but could be structural given its location on the weight-bearing side of the mummy. At the humeral midshaft, approximately 7 linen layers are counted in the 10-23 mm between the mummy's skin and layer ℓ1, and an additional 9 within the 20-28 mm separating layer ℓ1 and HPM4's external surface. Similar observations were made at the femoral midshaft and at the tibial midshaft. Approximately 57% of HPM4's volume is linen, and, using the typical spacing of the linen layer, an estimate of 7-8 m^2 of linen was obtained.[8] This represents an enormous expense.

3.8 Wires[9]

Thirty-six thin, linear and highly absorbing features connect to HPM4's surface, extend into the wrappings about 34 mm and are concentrated at the ends of HPM4 where linen curvature is greatest (Fig. 4a, 5). In the figures, the features were

identified as wires (i.e., specimen pins) because of the following reasons. These linear features do not appear to occupy any voxel completely, but x-ray absorption still approaches 1,000 HU, consistent with 0.5 mm diameter specimen pins. A diffraction pattern typical of the three wires encountered appears in Fig. 11a and consists of three strong diffraction lines. Each wire pattern appears only at a single *Y* position within a vertical scan across HPM4, and one of the *Y*-scans intercepted two wires. The origins of the pair of wire patterns match the positions seen in the CT section at the same position of the *Y*-scan (Fig. 9b). The wire diffraction lines possess the strong azimuthal intensity variation characteristic of the crystallographic texture of formed metals,[11] and precisely match peak positions and azimuthal intensity variation from a reference pin scanned separately from HPM4 (data not shown). The reference pin was a modern dual phase steel consisting of austenite and ferrite phases matching reference patterns (PDF 00-033-0397 and 00-006-0696, respectively). The wires within HPM4 were, therefore, added well after excavation, and such wire-based repair is commonly observed in CT scans of Egyptian mummies.[20]

3.9 Inclusion F

Inclusion F lies in the wrappings on the ventral side of the abdomen at the level of the lower lumbar spine (Fig. 4c) and is ellipsoidal with principal diameters of 7, 5 and 3 mm with the longer dimensions parallel to the wrapping planes and with the longest dimension along the cranial-caudal anatomical axis. This suggests the inclusion was purposely placed and was not a random piece of debris. Inclusion F is highly attenuating (3,055 ± 24 HU, near the scan's maximum), and, based solely on attenuation, one might identify the inclusion as garnet or malachite.[10] Anticipating the diffraction results, inclusion F is calcite which is listed at ~2,650 HU,[10] but it is not surprising that this difference was observed because the clinical scanner settings and software are not tuned for materials which are this absorbing.

Figure 11b shows a portion of a diffraction pattern for inclusion F. The pattern of six lines is representative of all of the other patterns from this inclusion, and lines 1-4 of Fig. 11b are identified in the figure caption along with their *d*-spacings. The diffraction pattern matches calcite (PDF 00-005-0586), albeit with slightly different lattice parameters. Inclusion F's diffraction lines contain many sharp, closely spaced spots with minimal radial broadening; this indicates fine grains with micrometer sizes. Diffraction patterns from inclusion F were observed over 7 mm translation along *X* and 5 mm along *Y*; the former matches that from the CT images and the latter is larger than what was measured in CT. Extrapolation to the calcite patterns originating volume agreed within 1 mm.[9]

Scarabs have been observed by CT of intact Egyptian mummies;[20, 22] two mummies have high absorption scarabs, somewhat larger than inclusion F and with somewhat lower absorptivity, on the abdomen at the lumbar vertebral levels.[20] Calcite amulets are unusual but not unheard of in mummies,[23] and the positioning of inclusion F above the abdomen is consistent with placement to protect (spiritually) the site of evisceration.[13] Much higher resolution CT would be required to show whether or not inclusion F possessed the shallow grooves defining the different parts of the scarab.

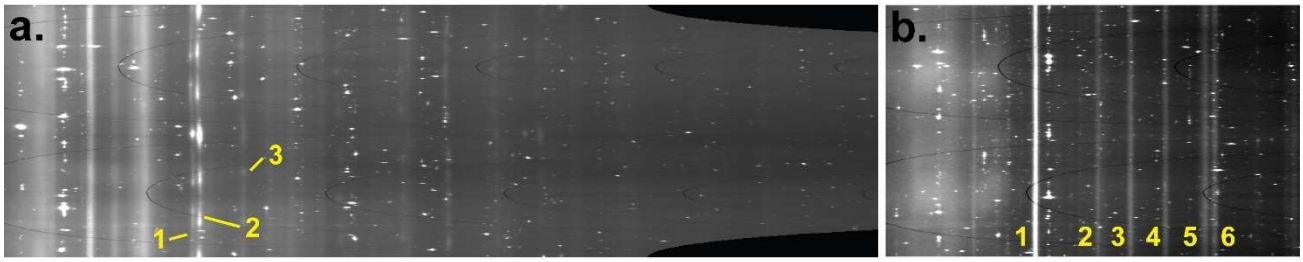

Fig. 11. Cartesian transformed diffraction pattern with the azimuthal axis vertical and radius horizontal; note that very different radial ranges are shown in the two panels. (a) Diffraction pattern from one wire. The austenite line 1 had d_{111} = 2.090 Å and 2.094 Å for the two wires encountered by the *Y*-scan and line 3 had d_{200} = 1.812 Å and 1.819 Å for the two wires. Diffraction line 2 was from ferrite and had d_{110} = 2.049 Å and 2.053 Å for the two wires. (b) Six strong diffraction lines from inclusion F with the labels are to the left of each line, except for line 6. The first four lines have *hk.l* indices 10.4, 11.0, 11.3 and 20.2 and values of *d* = 3.019, 2.483, 2.273 and 2.086 Å, respectively, which match calcite, specifically composition $Ca_{1-x}Mg_xCO_3$ with $0.03 < x < 0.06$ and closer to the lower value (PDF PDF 00-005-0586 and 00-086-0306). This composition of calcite matches that of local quarries operating when HPM4 was made.[21] Adapted from [9].

On the other hand, other highly absorbing particles exist elsewhere within the wrappings. Inclusions q1 and q2 have contrast ~2,000 HU, and x-ray diffraction identifies q1 as calcite. Certain portions of layers within the wrappings contain high attenuation particles ranging up to several mm in size. Some are well dispersed and other are closely spaced.[9] One suspects that q1, q2 and several other inclusions with similar contrast are limestone debris, mainly calcite with admixture of variable amounts of other, less absorbing mineral phases.

3.10 Conclusions about HPM4 and future directions

The CT scan showed that the person within HPM4 was about five years old at death, allowed the team to infer female biological sex and showed no evidence of skeletal trauma. Via CT, shards within the skull cavity were identified as solidified resin; linen layers were resolved wrapping the mummy, one of which appeared to be heavily impregnated with bitumen or pitch. Via CT and diffraction, wires (specimen pins), apparently added during earlier restorations of HPM4, were identified as a modern dual phase steel matching a reference specimen pin; a large, high attenuation inclusion located in the wrappings above the abdomen was identified as calcite, and one speculates that the inclusion is a scarab; the cross-sections of bones could be accurately mapped.

The combined CT and diffraction study showed that the CT data provided an extremely useful 3D "roadmap" guiding the diffraction experiments, the first of their kind performed in situ on an intact mummy. A ray tracing technique was developed to identify where along the x-ray beam path diffraction signals originated, and in all of the cases, origins matched positions of features identified in the CT scan within 1-2 mm. The desire to minimize potential beam damage to HPM4 dictated that very short integration times were used and the signal to noise was too low for detailed analysis of the bone diffraction patterns. The CT plus diffraction approach to studying the contents of mummies adds very important information, but the logistics of transporting a mummy first to a CT scanner and then to a synchrotron radiation source mean that the approach will probably only be used to solve key mysteries.

Application of fiducials placed on mummy prior to CT scan would help speed data acquisition and only deliver dose where there is a specific object of interest. From the CT data set, the fiducial's position would be measured relative to landmarks within the mummy. The fiducial would be found via scanning the x-ray microbeam and obtaining diffraction patterns from the fiducial with the beam off of the sample. One could then move to the position of interest, collect a coarse scan of short exposures to exactly locate the feature of interest and then collect a pattern at the position of interest with much longer count times, i.e., with very high signal to noise. This would limit any potential dose-related damage, a major concern in this first study, to a very localized volume. In the present instance, longer scans would not be required for features like the wires or inclusion F but would be used for studying bones where the patterns reported did not allow full analyses.

In order to confirm/refute the identification of inclusion F as a scarab, one must have voxel sizes small enough to detect the pattern of carvings on the surface of the object. In the author's opinion, this would require CT data sets with isotropic voxels on the order of 50 μm in size. This prospect is unlikely with clinical CT systems. As shown in Fig. 12, a local tomography approach[24] with an industrial (lab) microCT scanner lab could be used to detect the carvings on a putative scarab within a mummy. The caption to Fig. 12 gives the specifics. Industrial scanners are often located in shielded rooms which could accommodate objects much larger than HPM4. In this circumstance, HPM4 would stand on its feet, so to speak, a position in which HPM4 was on display for much of its post-excavation history,[6] within a supporting box and mounted on a rotation stage. Industrial scanners are often equipped with sample rotation stages easily able to accommodate the weight and diameter of HPM4. The diameter of the reconstructed local volume in Fig. 12 is 100 mm, about one-third of the largest dimension of the cross-section; the author has previously performed local tomography the reconstructed diameter being one-sixth the total diameter.[25]

The CT plus diffraction approach to studying the contents of mummies adds very important information, but the logistics of transporting a mummy first to a CT scanner and then to a synchrotron radiation source mean that the approach will probably only be used to solve key mysteries.

ACKNOWLEDGEMENTS

The author thanks: his collaborators M.K. Stock (Metropolitan State Univ. of Denver) and J.D. Almer (APS) for their important work leading to the complete scientific description of the study of HPM4;[9] the Styberg Library, Garrett-Evangelical Theological Seminary for allowing the studies on HPM4; the members of the Block Museum who facilitated

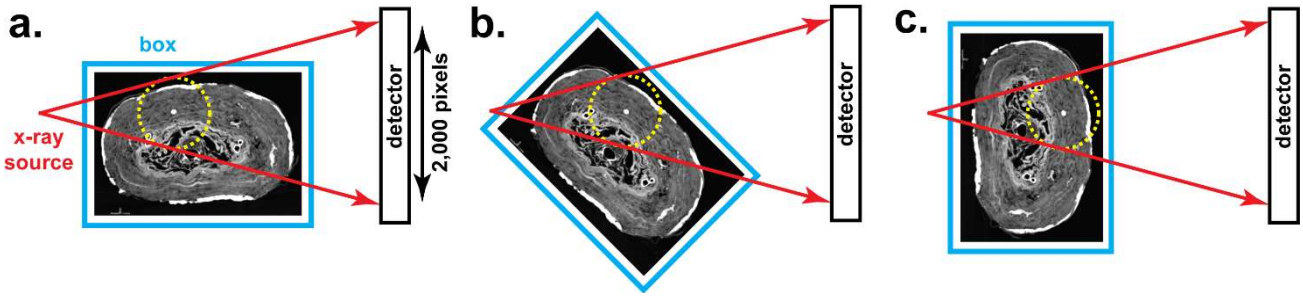

Fig. 12. Local tomography for producing reconstructions with 50 µm isotropic voxels within a 100 mm diameter volume surrounding inclusion F which is located at the center of the yellow dotted circle. (a-c) show the mummy at 0° rotation, 45° clockwise (CW) rotation and 90° CW rotation, respectively. The CT rotation axis is vertical and is centered under inclusion F. A low absorption support system (cyan, "box") holds the mummy upright. The x-ray source projects through the object and to the detector (red arrowed lines). The material within the 100 mm diameter yellow dotted circle always remains in the beam and projected onto the 2,000 pixel-wide detector.

the diffraction experiments and the curators of the exhibit "Paint the Eyes Softer" who enabled the study. This research used resources of the Advanced Photon Source, a U.S. Department of Energy (DOE) Office of Science User Facility, operated for the DOE Office of Science by Argonne National Laboratory under Contract No. DE-AC02-06CH11357.

REFERENCES

[1] Rönkkö, E., Terpstra, T., Walton, M. (Eds). [Portrait of a Child: Historical and Scientific Studies of a Roman Egyptian Mummy] Block Museum of Art, Northwestern Univ.: Evanston (IL) (2019).
[2] Freidrich, W., Knipping, P., and Laue, M. "Interferenz-Escheinungen bei Röntgenstrahlen," Sitzungb k Bayer Akad Wiss math-phys Klasse pp 303-322, 363-373 (1912).
[3] Bragg, W.L. "The specular reflection of x-rays," Nature 90, 410 (1912) and "The Diffraction of Short Electromagnetic Waves by a Crystal," Proc Camb Phil Soc 17, 43-57 (1913).
[4] Radon, J. "Über die Bestimmung von Functionen durch ihre Integralwerte längs gewisser Mannigfaltigkeiten," Berich Sächs Akad Wiss 69, 262-277 (1917).
[5] Rönkkö, E., Terpstra, T., Walton, M. "Introduction: A Roman Egyptian mummy from Hawara," in [1], 20-29.
[6] Corcoran, L.H. "From Egypt to Evanston: The modern afterlife of a portrait mummy," in [1], 82-93.
[7] Mininberg, D. "The Museum's mummies: An inside view," Neurosurg 49, 192–199 (2001).
[8] Stock, S.R., Stock, M.K., Dill, O., Almer, J.D. "Sex, age and mummification practices: Evidence from 3D X-ray imaging and x-ray diffraction," In: [1], 72-80.
[9] Stock, S.R., Stock, M.K., Almer, J.D. "Combined Computed Tomography and position-resolved x-ray diffraction of an intact Roman-era Egyptian portrait mummy," J Royal Soc Interface 17, 20200686 (2020).
[10] Gostner, P., Bonelli, M., Pernter, P., Graefen, A., Zink, A. "New radiological approach for analysis and identification of foreign objects in ancient and historic mummies," J Archaeol Sci 40, 1003-1011 (2013).
[11] Cullity, B.D., Stock, S.R. [Elements of X-ray Diffraction, 3rd ed.] Prentice-Hall, New York (2001).
[12] Gates-Rector, S.D., Blanton, T.N. "The Powder Diffraction File: A Quality Materials Characterization Database," Powder Diffraction 34, 352-60 (2019).
[13] Wade, A.D., Nelson, A.J. "Evisceration and excerebration in the Egyptian mummification tradition," J Archaeol Sci 40, 4198-4206 (2013).
[14] Alqahtani, S.J., Hector, M.P., Liversidge, H.M. "Brief communication: The London atlas of human tooth development and eruption," Am J Phys Anthropol 142, 481-490 (2010).
[15] Davey, J., Stewart, M.E.B., Drummer, O.H. "The value of CT imaging of Horus in determining the method of mummification and the sex of the mummy," J Med Imaging Rad Oncol 57, 657-662 (2013).
[16] Dill, O. "Interior and exterior: The function and production of mummy portraits in relation to the mummification process." In: [1], pp 94-99.
[17] Vahey, T., Brown, D. "Comely Wenuhotep: Computed Tomography of an Egyptian mummy," J Compu Asst Tomog 8, 992-997 (1984).

[18] Wade, A.D., Nelson, A.J., Garvin, G.J. "A synthetic radiological study of brain treatment in ancient Egyptian mummies," HOMO – J Compar Human Biol 62, 248-269 (2011).
[19] Hawass, Z.A., Saleem, S.N., D'Auria, S. [Scanning the Pharaohs: CT Imaging of the New Kingdom Royal Mummies] American University in Cairo Press, Cairo-New York (2016).
[20] Raven, M.J., Taconis, W.K. [Egyptian mummies: Radiological atlas of the collections in the national museum of antiquities in Leiden] Brepols, Uurnhout, Belgium (2005).
[21] Aston, B.G., Harrell, J.A., Shaw, I. "Stone," in: P.T. Nicholson, I. Shaw (Eds.) [Ancient Egyptian Materials and Technology] Cambridge University Press, Cambridge (2000) 5-77.
[22] Jansen, R.J., Poulus, M., Venema, H., Stoker, J. "High-resolution spiral CT of Egyptian scarabs," RadioGraphics 22, 63-66 (2002).
[23] Rijksmuseum van Oudheden collection: https://www.rmo.nl/collectie/collectiezoeker/collectiestuk/?object=15141, accessed April 15, 2020.
[24] Stock, S.R. [MicroComputed Tomography: Methodology and Applications, 2nd Ed.] Taylor and Francis, Boca Raton (2019).
[25] Stock, S.R., Veis, A., Xiao, X., Almer, J.D., Dorvee, J.R. "Sea urchin tooth mineralization: Calcite present early in the aboral plumula," J Struct Biol 180, 280-289 (2012).